The Influence of Burner Surface Morphology on Flame Stabilization

Safira da Silva Braz

safira.braz@tecnico.ulisboa.pt

Instituto Superior Técnico, Universidade de Lisboa, Portugal

November 2018

Abstract

The present study asses about the potential application of a porous material in lamella-type burner in lean conditions, which are widely used in domestic heating devices. The porous morphologies were produced from zinc oxide (ZnO) and a detailed investigation about the inverted flame stabilization was carried out. ZnO materials with different types morphologies (non-porous and porous materials) were produced using an electrodeposition technique. These materials have been synthesized under specific growth conditions for a range of times, current densities and electrolyte solutions. The growth and morphology evolution of these materials were studied in detail and leaded to produce a three-dimensional (3D) structures with interconnected porosity. Temperature measurements of the plate surface and stand-off distances near the blow-off moment were taken in this experimental study. These were used to estimate a Peclet number and the heat flux in the region between the base flame and the plate, allowing to understand the conditions in which the flame extinguished, and determine the stability diagrams. The results show that for surfaces with porous diameter greater than 167 μm, occurs the flame blow-off for higher equivalence ratios (ϕ) when compared with a surface without deposited material. Particularly it has been recorded a change in the velocity profile for lower velocities (U< 1,71 m/s). This variation forces the approximation of flame base to the ZnO surface, a new stabilization occurs and consequently an increase of the heat transfer to the ZnO material.

Keywords: Porous materials, Zinc Oxide, Flame Stability, Thermographic Camera, Lean Combustion

1. INTRODUCTION

The worldwide concern about greenhouse effects have pushed industries relying on hydrocarbons combustions to improve their processes and reduce emissions [1]. To this end, new combustion areas has appearing such as lean combustion and micro combustion, since working with a lower flame temperatures NOx emission are reduced [2]. However, both brings limitations since promote poor flame stability which might compromises the device operation.

Micro combustion has been suffering from a growing trend, especially due to the rising demand for portable power generation suitable to use in micro air vehicles or in communication devices [3]. These types of portable devices strongly rely on batteries, which have a very low energy density, lack of compact, lifetime and light weight. Due these limitations, hydrocarbon's fuel appears as an alternative since they have a very high specific energy (45 MJ/Kg over 1,2 MJ/Kg of the lithium batterie) [4]. Additionally, this scale down carries out news challenges, particularly on the micro chamber. As combustion volumes are reduced, issues of residence time, heat losses, air/fuel mixing and flame quenching become significantly relevant [5]. Surface-induced catalytic reaction has shown significant improvements in sustainable combustion in micro combustion. Coating the wall surface of a combustor with a proper catalyst can lower the reaction activation energy enhancing the reaction rate in low temperatures. Consequently, the lower temperatures enabled in the process will allow NOx emission reduction [5].

In the case of methane (CH_4) combustion, metal oxides (as Co_3O_4, $ZnCrO_4$ and $CuCrO4$) and noble metals such as Pt, Rh and Pd have been tested and used as a promotor for catalytic oxidation of CH_4 [6]. Also, the catalysts are usually dispersed on a support. This support substrate has a porosity above 50% and

a high surface area, required characteristics for the catalytic combustion. Monoliths and ceramic honeycombs are examples of support materials used for methane catalytic reaction [6,7,8]. The support substrate plays a relevant role on the catalytic reaction, since it might influence the activity and long-term stability of the catalysts [6] and also offers high combustion efficiencies [5]. Such features are favourable for catalytic combustion application for sustaining flame in a smaller volume.

The domestic heating industry relies heavily in exposed combustion approaches – lean and micro combustion. An example, used in house water heater equipment's, is the lamella type burner (see Figure 1). This technology is characterized by the combination and interaction of small-scale inverted flames [9,10]
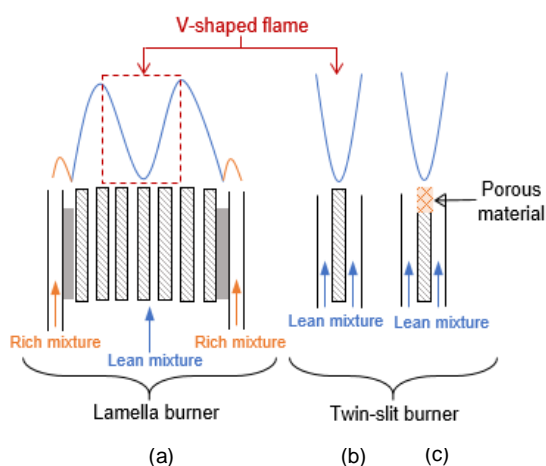

Figure 1 – Inverted flames applications: (a) lamella burner, (b) twin-slit burner and (c) twin-slit burner with porous material applied. Adapted from [9].

Inverted flames burners were firstly used by Lewis and von Elbe [11], using a wire mounted in the axes of a cylindrical burner tube, and later by Edmondson and Heap [12], using stabilized V-flames and twin-slit burners in thin plates of different thicknesses, as seen in Figure 1.

In relation with catalytic combustion on domestic heating industry, works are only found which take natural gas boilers using a metal honeycomb partly coated with a catalyst [13]. However, these researches are focussed on the catalyst influence in combustion rate and less over the importance of the support material.

This study attempts to look at the potential application of catalytic surfaces in lamella burners (Figure 1), in particularly for household heating market where there has been limited research. The focus has been in understanding how a porous catalyst might influence the flame behaviour, rather than looking at methane catalyst coatings. At this small scale, the morphology of a support material is of an extreme significance as the pore dimensions may introduce undesired instabilities in the flame, even with the impregnation of methane catalysts.

Study of the support morphology was achieved by producing a material with a 3D interconnected porosity, similar as the support material catalyst [8]. Zinc Oxide (ZnO) was used to synthesize the porous materials due to its low cost, high availability and low toxicity [14]. Electrodeposition as used to fabricate the porous structures as offered a simple, fast and low-cost process [15]. Direct visualization and temperature measurements were performed in order to assess about the influence of a porous material in the flame holder.

2. EXPERIMENT

2.1 BURNER SET-UP

Figure 2 shows the experimental setup. The system was feed by two main streams, one of methane (CH_4) and another of air. The methane was supplied by a high-pressure cylinder and the air removed directly from the atmosphere, passing by an air filter to ensure the removal of impurities and water before continuing its course. Each stream was connected to a digital flowmeter. After passing through the flow controllers, both air and methane streams were mixed and plugged to the twin-slit burner (Figure 3). This scheme allows the user to control both flow meters imposing the equivalence ratio (ϕ) as well the velocity at burner exit (U).

It should be emphasized that the plates used in burner tests were plates coated with synthesized ZnO porous materials. Tests were also performed with a clean stain steel (SS) plate used as a reference sample for comparison with produced materials.
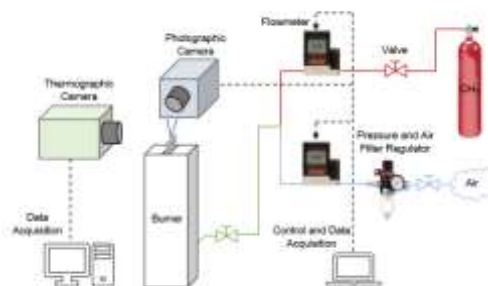

Figure 2 – Scheme of the experimental set up.

The burner used was a two-dimensional slit burner with two rectangular channels with equal geometry of size 40x2 mm (Figure 3). The flame was stabilized behind the trailing edge of a plate with a 3mm thickness, which was positioned a 13 mm above the burner exit (Figure 3). This type of burner configuration allows to produce and isolate a V-shaped flame, giving improved optical access during experiments.
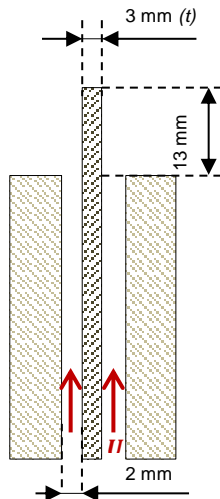

Figure 3 – Cross-section of the burner.

2.2 PROCEDURE

All tests started with a fixed flow velocity (e.g. Re=100) and a ϕ=0.7. The parameter ϕ was then reduced in intervals of 0.01 allowing the flame to stabilized in the new condition (about t=15s). The decrements were performed until the flame extinguished, representing the all the obtained results as the moment before the blow-off limit with $\phi_{data} = \phi_{blow-off} - 0.01$. This process was repeated several times for each flow velocity (Re range 100-700), to check against reproducibility of results.

2.3 TEMPERATURE MEASUREMENT SET-UP

Figure 4 shows the experimental setup used for temperature measurements. The temperatures were measured using a ONCA 4969 infrared (IR) thermographic camera from Xenics, operating at the temperature range of 40-400˚C.

The temperatures measured correspond to a single point/pixel in the top edge of the plate, as illustrated in Figure 5. The camera was facing the lateral side of the flame holder and positioned in a stale and safe location close to the burner.

It was needed to use a black surface to cover up the flame and avoid flame radiation to the lens. With this strategy, it was possible to distinguish the flame base

from the plate, allowing to choose the same pixel position along the various experiments using the camera's software.

Due to the small plate thickness (t=3mm) it was assumed that the plate behaves as an extended surface with a linear temperature distribution along
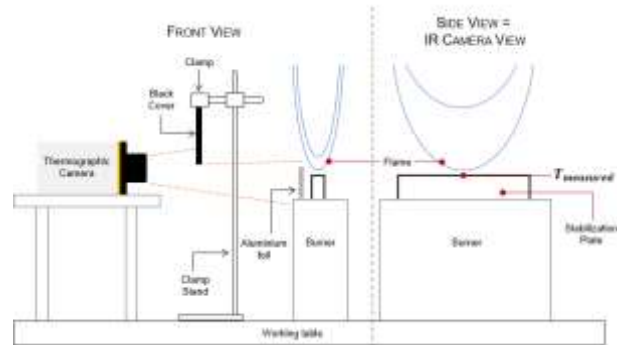

Figure 4 – Scheme of the experimental set-up for temperature measurements.
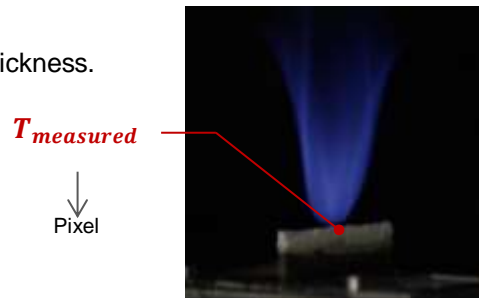
the thickness.

Figure 5 – Location where the temperature values were measured.

2.4 STAND-OFF DISTANCES

Canon EOS 7D was used to inspect the flames' behaviour, namely the flame profile. An image processing using a MATLAB® routine was performed in order to assess about the flame displacement. Figure 6 shows the steps used to analyse the stand-off distances.

The reference used to define the real position of the flame from the stabilization plate was a target with millimetric paper and the scale of conversion from pixels to mm unity was performed using *ImageJ* software. Briefly, the procedure consists in a conversion from an RGB image to a BW,
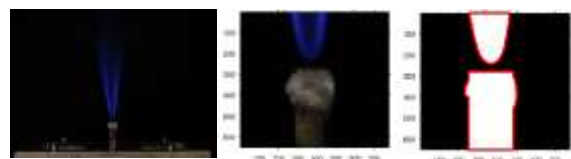

Figure 6 – Post processing adopted to evaluate the stand-off distance.

boundaries definition and compute the stand-off distance. This value corresponds to the subtraction of the highest pixel from the boundary of the flame and the lowest pixel from the flame holder. This value is multiplied by the conversion factor.
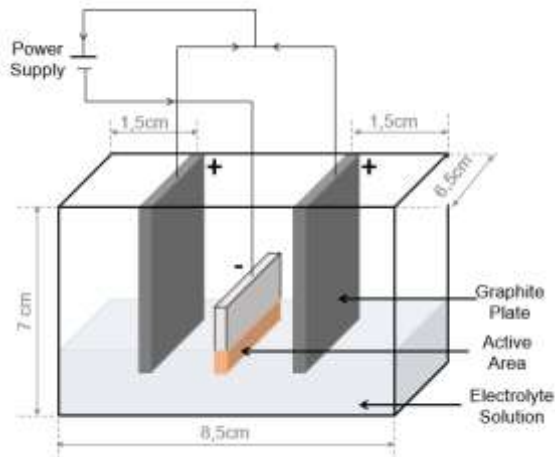

Figure 7 – Electrodeposition set-up.

2.5 ZnO Materials

The ZnO materials were produced using the electrodeposition technique by Dynamic Hydrogen Bubble Template (DHBT). The name arises from the fact that when applied the right potential (or current) a dynamic template can be obtained, since during the electrodeposition process H^+ is reduced to H_2, producing H_2 bubbles that interfere on solid growth mechanism. This spontaneous process occurs during the metal deposition which allows to produce easily porous morphologies [15].

Figure 7 presents the electrodeposition apparatus. Two types of electrolytes solutions (A and B) were used, differing each other only in the presence of the supporting electrolyte KCl as shown in Table 1. Electrodeposition was carried out in galvanostatic mode by applying a current density (i) of 0.1 to 0.4 A cm^{-2} for 60 and 90 s. After experiments, all depositions were rinsed with ethanol and taken into an oven at 500˚C for 5 hours, for a thermal oxidation. Analytical grade chemicals and distilled water were used to prepare both solutions.

Table 1 – Electrolyte solutions composition

Electrolyte	$ZnCl_2$ (Sigma-Aldrich)	NH_4Cl (Sigma-Aldrich)	KCl (Sigma-Aldrich)	pH T=20.5˚C
A	0.5	0.5	2.0	4.88
B	0.5	2.0	-	4.35

2.6 Mean Pores Diameter Estimation

Figure 8 shows the sequence of SEM micrographs post processing carried out to estimate the mean pores dimension of the porous materials tested on the burner. It was used an algorithm developed in MATLAB® R2017b software, applying features from the image processing toolbox as the Euclidean distance transform and the watershed transform (Gonzalez and Woods [16]).
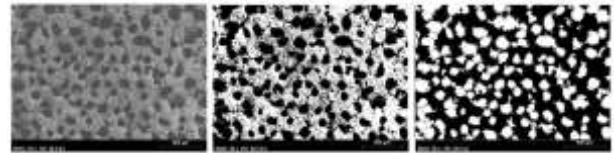

Figure 8 – Procedure used to evaluate pores dimension

3. Results

3.1 ZnO Materials
3.1.1 Characterization of ZnO Materials

Figure 9 shows the X-ray diffractograms (XRD) of ZnO materials produced from electrolyte A. The XRD of the ZnO materials showing diffraction peaks in the 2Ɵ range 10⁰–70⁰, corresponds to the characteristic reflections of zincite (ZnO) (RRUFF ID: R050419) [17] structure. The two peaks identified with the red dashed lines can be assigned to KCl impurities, since these peaks found at 28.5˚ ad 40.8˚ agree with those found in RRUFF data base for sylvite, KCl (RRUFF ID: R050166) [18].
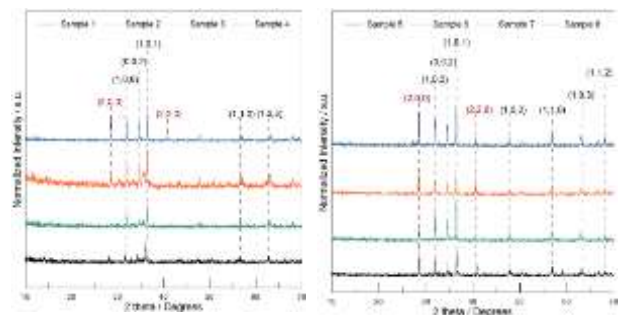

Figure 9 – X-ray diffractogram for electrolyte A. The left side corresponds to t=60s and the right side to t=90s.

The SEM micrographs presented in Figure 10 and Figure 11 show the evolution of the synthesized ZnO materials evidencing the formation of a porous structure under higher i (i>0,3 A.cm^{-2}) and longer deposition times (t), The six porous materials highlighted in Figures 10 and 11 with red lines were the ZnO material selected to perform the flame stabilization tests. Due to the DHBT

method, with higher i occurs an increase of the bubbles density originating pores with the same dimension as the diameter of the released bubbles [15]. A 3D structure with interconnected porosity was produced in both electrolytes (A and B) for the same electrodeposition conditions: t=60s+i=0.4 A cm^{-2} and t=90s+i=0.3 and 0.4 A cm^{-2}.

Figure 12 and Figure 13 present the chemical composition (at atomic weight %) detected by EDS of all produced material. Regarding to EDS for electrolyte A (Figure 12), a decrease on Zn (red line) detection is observed and a parallel increase of Cl an K elements (green and orange lines, respectively) along increments of i. This is due to the formation of KCl crystals which covers more surface and consequently leads to the reduced emission of Zn. It is evident an increase of K and Cl curves, which nearly overlap, evidencing the growth of KCl crystals.

Regarding electrolyte B (Figure 13), EDS shows the same order of magnitude of the Zn element in the composition of all produced samples (between 80 and 95% in atomic weight), without showing any trend with the manipulated parameters (time and i).

The small values of chemical element O in both electrolytes is because of its weight. Since O is light element with a poor vibration when excited, the equipment can't detect its emission.

The obtained results from XRD and SEM/EDS confirm the formation of ZnO as intended in all synthesized material. Also, longer electrodeposition times and higher i allowed to produce material with a 3D porosity structure with different pores dimension to use in the burner.

3.1.2 AVERAGE PORES DIMENSION

From Figure 14 it is possible to infer that electrolyte A provides a wider range of pores sizes when comparing with electrolyte B. Also, the porous materials produced with higher i have larger pores: for instance, D_m (7A) is smaller when comparing with D_m (8A), both having the same deposition time (90s) but different i. The measured D_m values are within the range reported in literature [19] for this type of surfaces.
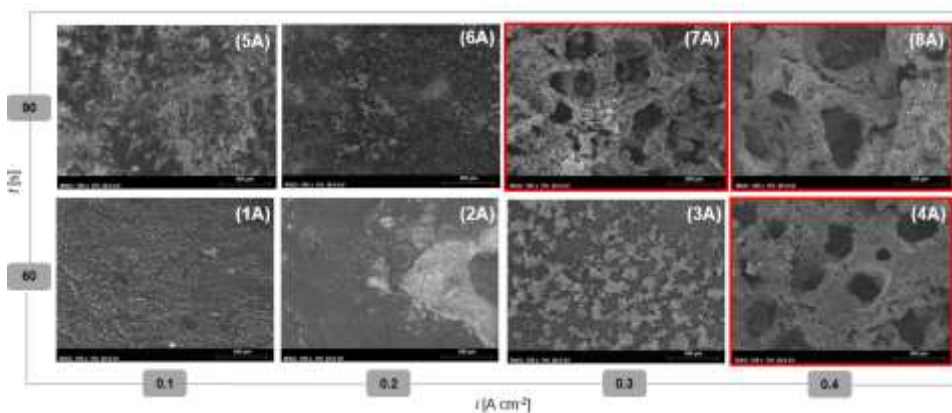

Figure 10 – SEM micrographs of synthesized samples according t and i for electrolyte A.
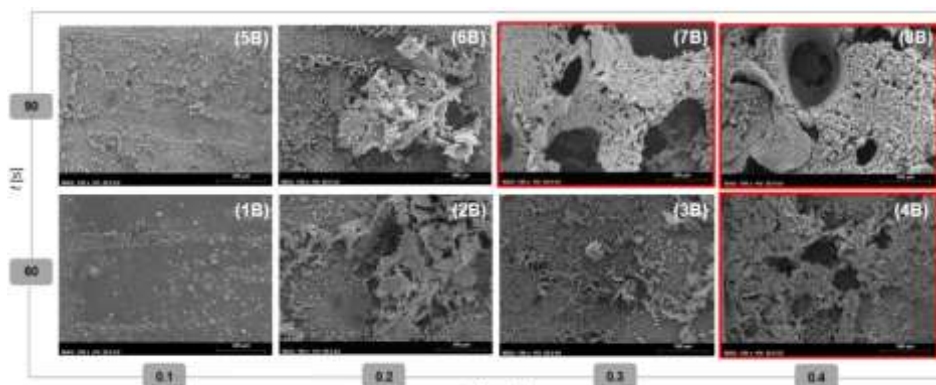

Figure 11 – SEM micrographs of synthesized samples according t and i for electrolyte B.
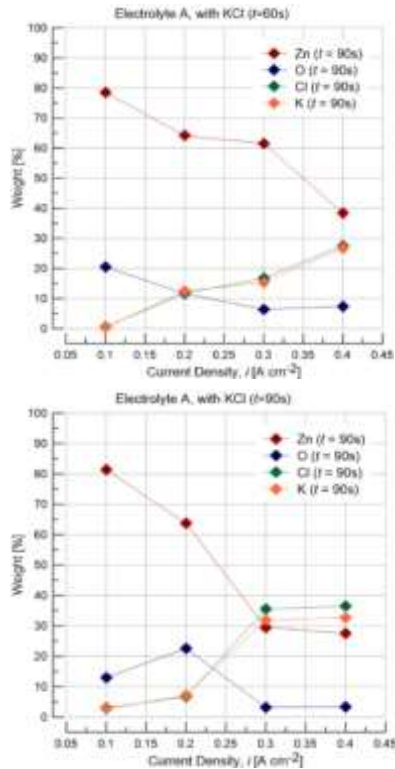
Figure 12 – Evolution of the chemical elements present in synthesized ZnO materials for electrolyte A (w/ KCl) for (a) 60s and (b) 90s electrodeposition times.
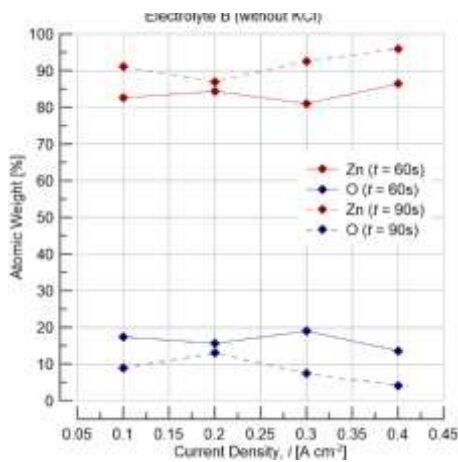

Figure 13 – Evolution of the chemical elements present in synthesized ZnO materials for electrolyte B (w/o KCl) for (a) 60s and (b) 90s electrodeposition times.

The presence of KCl in electrolyte solution (see sample 4 for instances) provides a bigger pores formation due to the accelerate growth mechanism [19,20].

3.1.3 BEFORE AND AFTER COMBUSTION TESTS

Comparing the before and after images of the porous samples in Figure 15 it can be seen that only electrolyte A remained the porous structure. It is believed that the presence of KCl in solution A may influence the formation of intrinsic defects by

changing the morphology of the deposited material as demonstrated by Tena-Zaera et al [21], leading to the synthesis of a firmer surface. Electrolyte B loses completely its porosity structure, leading to a poor and delicate material,
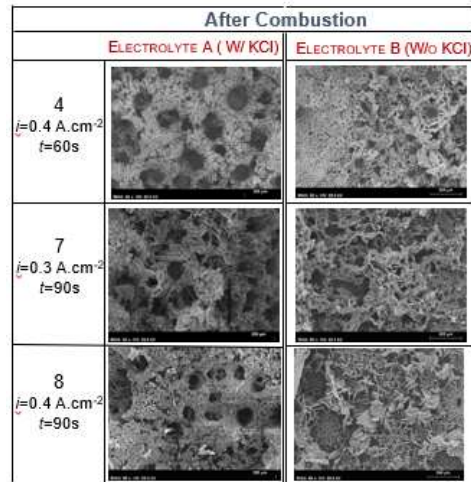

Figure 15 – SEM micrographs after burner' experiments of ZnO porous materials

and making it unsuitable for this type of application. However, besides the produced material are being delicate and needed to be handled with care, visually there is no degradation of the material.

3.2 COMBUSTION

3.2.1 LEAN STABILITY DIAGRAMS

The flame stability criterion was defined as the blow-off moment, since before achieving this limit the flame is a well-defined and stable V-shape. Once the flame extinguished, the conditions of this blow-off moment were recorded in the flowmeter's software. Each condition was performed several times in order to check against reproducibility. Figure 16 and Figure 17 shows the stability limits obtained for all the six-porous ZnO materials tested. The black square data points refer to a clean stabilization plate without material deposited (SS plate) and is used as a reference measurement. The values measured for the reference holder are in the same order of magnitude with those found in literature [22]. For low flow velocities it can been seen that all porous materials have an opposite effect on the flame stabilization, since the blow-off occurs at higher ϕ which is not a desirable behaviour. However, the porous material tends to have the same action as the clean surface with an increase of mixture velocity, allowing an approximation of all stability curves to the
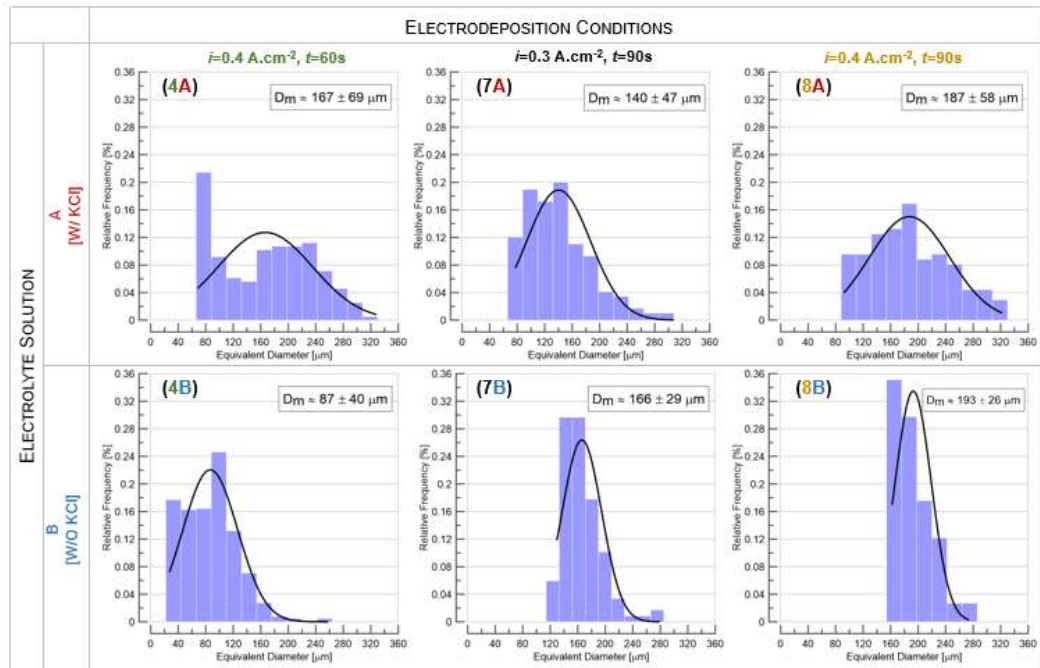
6

Figure 14 –Pores size distribution.

reference curve. Notice that for electrolyte A (Figure 16) the ZnO material with smaller pores (green curve, Dm ≈ 140μm), when compared with the other produced materials with bigger pores, has a similar trend as the reference curve (black line).

In addition, it is visible a higher displacement of the electrolyte B curves comparing with electrolyte A from the reference curve. This is due to the ZnO porous material produced with electrolyte B losing completely their morphology as shown in after combustion SEM micrographs (Figure 15). The deposited mass led to a difficulty in flame stabilization. This result verifies the importance of KCl role in the process, since its presence allowed to preserve the flame at lower ϕ. Since the electrolyte B samples lost its the porous structure, from now on it will presented

only the results obtained for materials synthesized from electrolyte A.

3.2.2 TEMPERATURE MEASUREMENTS

The temperatures measurements were performed in one pixel in the top side of the flame holder (see Figure 5).

Figures 17, 18, 19 and 20 present the measured temperature profile from ϕ =0.7 to the flame extinction for a range flow velocities for Re=100-700. The end left points for each line of flow velocity correspond to the near flame blow-off (BO) limit, i.e., $\phi = \phi_{BO} - 0.01$. Observing the temperature results, 4A and 7A ZnO materials are the samples that present a smoother/linear temperature variation along ϕ decrements.
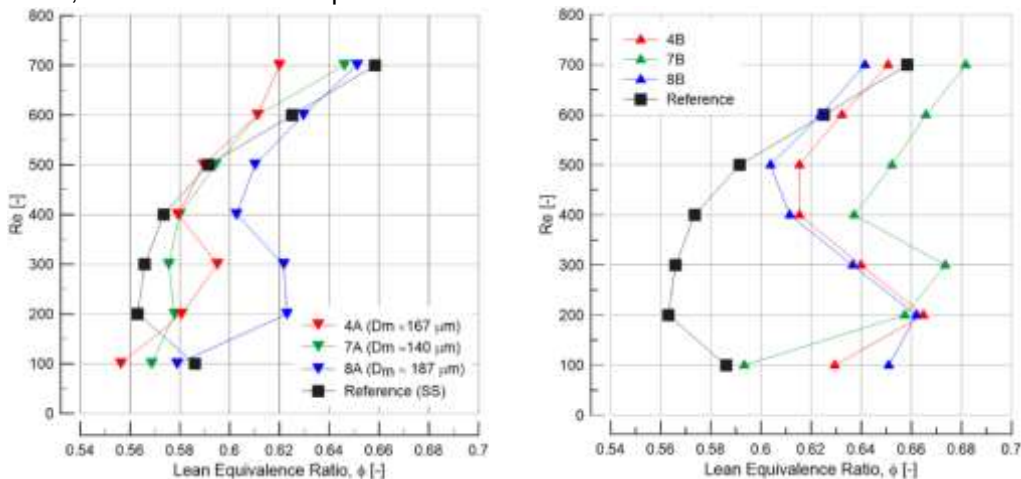

Figure 16 – Lean Stability Diagram obtained for ZnO porous materials produced from electrolyte A (left) and from electrolyte B (right side).
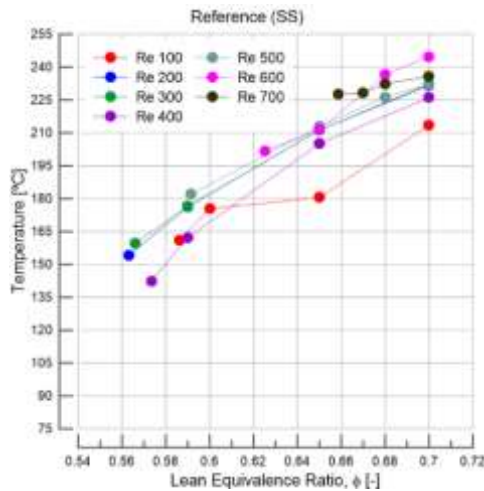
7

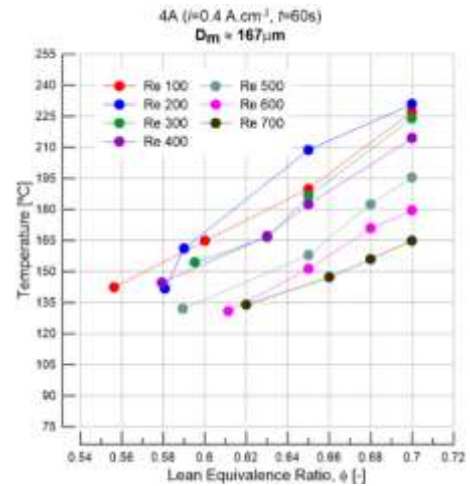Figure 17 – Temperature evolution measured for SS plate.

Figure 18 – Temperature evolution measured for sample 4A.

Figure 19 – Temperature evolution measured for sample 7A.

Figure 20 – Temperature evolution measured for sample 8A.

Oppositely, the remain samples have prominent slopes, with a noticeably reduction of the temperatures near the blow-off state. For instance, observing the Re 300 green curves, the temperature measured near blow-off limit for both 4A and 7A was around 150˚C, although for sample 8A this value drastically decreased to approximately 90˚C. Also, this temperature results for samples 4A and 7A are similar to the reference (Figure 17) corroborating the approach of the stability diagrams seen in Figure 16 of ZnO samples 4A and 7A to the reference.

Gathering this temperature and stability results, it is evident how important are the pores dimension in the flame stabilization, since materials with pores of a mean diameter of 167μm lead to a behaviour identical to the SS plate. Moreover, the positive slope observed in all temperatures curves is the result of the join of the follow effects: decrease of T_{ad} with ϕ, the heat and radical lost with the increase of flow velocity, and the $\bar{k}_{COND}$ of the mixture in the control volume between the base flame and the stabilization plate. According Olorunyolemi et al. [23] which studied the thermal conductivity of a micrometre ZnO particle ($\bar{k}_{ZnO \ (\mu m \ particle)} \approx 0.1 \ W/mK$ in a temperature range of 0-200˚C), it is possible to assume that the synthesized material has a smaller thermal conductivity relative to the SS ($\bar{k}_{SS} \approx 13W/mK$ [24]). As ZnO has a smaller $\bar{k}_{cond}$, it is expecting a decrease of the temperature.

3.2.3 HEAT FLUX

Concerning to the material where the flame is stabilized, the amount of energy that is being transferred by conduction (Q) and unit of time is known as Fourier's Law. Simplifying it is possible to assume the flame as a hot source that is

heating the stabilization plate, obtaining the follow equation

$$\dot{Q} = t_{FH} k_{mix} \frac{T_F - T_S}{d_s} \qquad (1)$$

where, $\dot{Q}$ is the heat flux, t_{FH} is the flame holder thickness, k_{mix} the thermal conductivity of fuel-air mixture, T_F is the flame adiabatic temperature, T_S the temperature of the plate surface and d_s is the stand-off distance.

Figure 21 shows the stand-off distances measured at incipient blow-off. Towards lower flow velocities (Re between 100 and 300), the flame base reaches close proximity to the plate with the ZnO materials. This result can be attributed to the pores size, which their dimension may be inferred from the velocity field forcing the approximation of the flame seeking for stabilization. Also, it is observed a constant stand-off distance for the reference plate (nearly a vertical curve as seen in the black curve of Figure 21), which varies between 1.5 and 2.0 mm in either flow velocity.

According to study carried out by Leitão [24] an almost constant velocity profile is reached through the porous material independent of the tested flow rates ($\bar{U} = 0.1$ m/s), which can help to understand the flame performance with this type of media. In fact, it is possible to conclude that this material (green curve in Figure 16) is an extension of the SS. Summarizing, materials with a pores with a mean diameter of 140μm don't create instabilities to the flame, which might suitable to work as support catalysts in future applications.

Figure 22 shows the heat flux calculated by Equation (1). It is observed a opposite behaviour of the ZnO material relative to the reference curve for lower flow velocities. Below Re = 400 the heat losses are higher than the reference (e.g. for Re=300, $\dot{Q}_{Reference} = 60$ W/m and $\dot{Q}_{7A} \approx 100$ W/m). Also, it was observed a displacement of the flame towards the plate, which increase the heat transfer to the plate. Notice that the higher $\dot{Q}$ values obtained for the porous material with small pores (7A, with D_m=140μm) might be assigned to the thermal conductivity of this type of material.

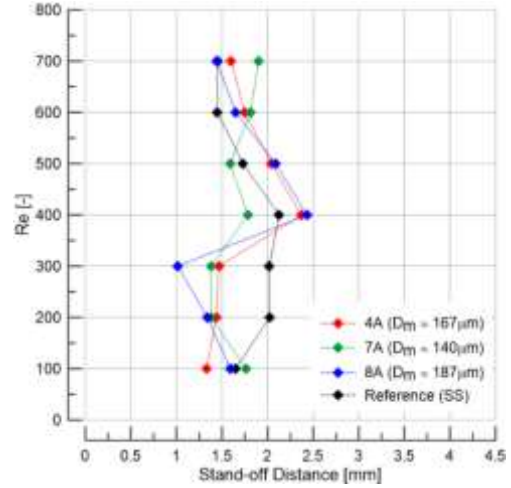For higher U, the $\dot{Q}$ curves of the ZnO material approach the reference line, producing the same

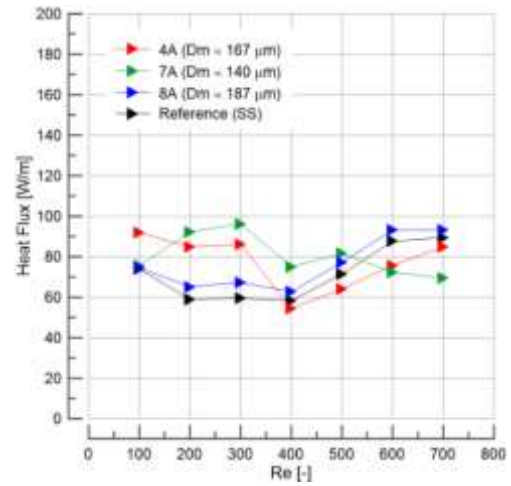Figure 21 – Stand-off distances (d_s) measured near blow-off limit

Figure 22 – Heat fluxes measured at incipient blow-off for the produced material from electrolyte A.

effect as the SS plate in flame stabilization, as confirmed by the stability diagrams.

4. CONCLUSIONS

Concerning to the synthesized ZnO material, XRD and the SEM micrographs show that ZnO samples were prepared successfully by electrodeposition. Also, the importance of KCl in the electrolyte solution was evaluated, showing that this is an important parameter to produce a stronger and resistant porous structure to perform tests in this type of twin-slit burners.

The experimental results fit into the hypothesis in which the pores size of the synthesized material changes the velocity profile at the trailing edge of the flame holders, particularly for small flow velocities. The main conclusions to be drawn with the surface manipulation at incipient blow-off of an inverted flame may be summarized as follows:

(i) A material with small pores (mean diameter from of 140 to 167μm) behaves as a clean flame

holder (no material deposition) given the similarities in the stability curves

(ii) The presence of a porous media does not promote any change of the flame stabilization for higher mixture velocities, since the flow does not seem to travel through the porous material.

(iii) The presence of a porous media changes the velocity profile at the trailing edge of the plate since a displacement of the flame occurs towards the flame holder, consequently increasing the heat transfer from the flame base to the stabilization plate, and leading to the flame blown off.

REFERENCES

[1] M.L. Williams and D.C. Carslaw. New Directions: Science and policy – Out of step on NO x and NO 2?, *Atmospheric Environment* 45: 3911–3912, 2011.

[2] D. Dunn-Rankin and P. Therkelsen. *Lean Combustion, Technology and Control*. Academic Press, 2nd edition, 2016.

[3] Y. Ju and K. Maruta. Microscale Combustion: Technology development and fundamental research. *Progress in Energy and Combustion Science*, 37(6): 669-75, 2011.

[4] Y. Nakamura, J. Gao and T. Matsuoka. Progress in small-scale combustion. *Journal of Thermal Science and Technology*, 12(1): 1-28, 2017.

[5] B. Bui. Micro-scale combustion issues and approaches. MSc thesis, California State University, 2013

[6] J.H. Lee and D.L. Trimm. Catalytic combustion of methane. *Fuel Processing Technology*, 42: 339-359, 1995.

[7] T. Heppenstal. Assessment of the impact of catalytic surface combustion on heat transfer in a tube. *Heat Recovery Systems & CHP*, 13(6): 483-492, 1993

[8] S. Govender and H.B. Friedrich. Monoliths: A Review of the Basics, Preparation Methods and Their Relevance to Oxidation. *Catalysts*, 7(62), 2017.

[9] S. Parmentier, M. Braack, U. Riedel and K. Warnatz. Modeling of combustion in a lamella burner. *Combustion Science and Technology.* 175(1): 185-206, 2003.

[10] T. Lúcio. Rich-Lean Flame Interaction on a Lamella Type Burner. MSc Thesis, Lisbon University, 2015.

[11] B. Lewis and G. Von Elbe, Stability and Structure of Burner Flames, *J. Chem. Physics*, 11: 75-97, 1943.

[12] H. Edmondson and M.P. Heap. Blowoff of Inverted Flames, *Combust. and Flame*, 14: 191-194, 1970.

[13] S.R. Vaillant and A.S. Gastec. Catalytic combustion in a domestic natural gas burner, *Catalysis Today*, 47: 415-420, 1999.

[14] Z. L. Wang. Nanostructures of zinc oxide, *Materials Today*, 7(6): 26-33, 2004.

[15] B.J. Plowman, L. A. Jones and S.K. Bhargava. Building with bubbles: the formation of high surface area honeycomb-like films via hydrogen bubble templated electrodeposition, *Chem. Commun.*, 51: 4331-4346, 2015.

[16] R.C. Gonzalez and R.E. Woods, Digital Image Processing Pearson Education Inc., 2nd Edition. 2008.

[17] http://rruff.info/Sylvite (May 2018)

[18] http://rruff.info/Zincite (May 2018).

[19] R. Tena-Zaera, J. Elias, G. Wang and C. Lévy-Clément. Role of Chloride Ions Electrochemical Deposition of ZnO Nanowire Arrays from O2 Reduction, *J. Phys. Chem. C*, 111(45): 16706-16711, 2007.

[20] A. Moezzi, M. Cortie and A. McDonagh. Transformation of zinc hydroxide chloride monohydrate to crystalline zinc oxide, Dalton Trans., 45, 7385-7390. 2016

[21] R, Tena-Zaera, J. Elias, C. Lévy-Clément, C. Bekeny, T. Voss, I. Mora-Seró and J. Bisquert. Influence of the Potassium Chloride Concentration on the Physical Properties of Electrodeposited ZnO Nanowire Arrays, *J. Phys. Chem.*, 112: 16318-16323. 2008.

[22] Y. Shoshin and L.P.H De Goey. On the Correlation of Inverted Flame Blow-Off Limits with the Boundary Velocity Gradient at the Flame Holder Surface, *Combust. Explo. And Shock Waves*, 5: 520-527, 2015.

[23] T. Olorunyolemi, A. Birnboim , Y. Carmel, Jr. O.C. Wilson and I.K. Lloyd. Thermal conductivity of Zinc Oxide: From Green to Sintered State, *J. Am. Ceram. Soc.*, 85, 1249-1253, 2002.

[24] F.P. Incropera, D.P.Dewitt, T. L. Bergman and A.S Lavine. Fundamentals of Heat and Mass Transfer, 6th ed., John Wiley & Sons, Hoboken.2007.

[25] I. Leitão. Experimental and Analytical Flame Transfer Functions of Multi-Perforated Plate Burners. MSc Thesis, Lisbon University, 2009.